Supporting Information

Finding a new pathway for acid-induced nitrite reduction reaction: formation of nitric oxide with hydrogen peroxide

Mohammed Ajmal P. Y.[||†] Somnath Ghosh,[||†] Mahesh Yenuganti, Yatheesh Narayan,[†] Munendra Yadav,[§] Subash Chandra Sahoo[‡] Pankaj Kumar*[†]

[†]Department of Chemistry, Indian Institute of Science Education and Research (IISER), Tirupati 517507, India

[‡]Department of Chemistry, Punjab University, Punjab, Chandigarh, India

[§]Department of Chemistry, University of Texas at El Paso, El Paso, Texas 79968, United States

* To whom correspondence should be addressed.

E-mail: pankaj@iisertirupati.ac.in

Table of Contents

Experimental Section

Materials. All reagents and solvents obtained from commercial sources (Sigma Aldrich Chemical Co. and Tokyo Chemical Industry) were of the best available purity and used without further purification unless otherwise indicated. Solvents were dried according to reported literature and distilled under inert atmosphere before use.[S1] $Na^{15}NO_2$ (99.2% ^{15}N-enriched) was purchased from ICON Services Inc. (Summit, NJ, USA). The 12-TMC ligand was prepared by reacting excess amounts of formaldehyde and formic acid with 1,4,7,10-tetraazacyclododecane as reported previously.[S2]

Instrumentation. UV-vis spectra were recorded on a Hewlett-Packard 8453 diode array spectrometer equipped with a thermostat cell holder (UNISOKU Scientific Instruments) designed for low-temperature experiments. FT-IR spectra in solid form were recorded on Bruker-Alpha Eco-ATR FTIR spectrometer using standard KBr disk method. The solution IR spectra were recorded on the Cary 630 spectrophotometer in the frequency range of 400 – 4000 cm^{-1} using demountable liquid-cell kit having round KBr cell window (32 mm). ^{1}H-NMR spectra were measured with a Bruker model Ascend 400 FT-NMR spectrometer. Electrospray ionization mass spectra (ESI-MS) were recorded on an Agilent Mass Spectrometer (6200 series TOF/6500 series Q-TOF B.08.00), by infusing samples directly into the source using a manual method. The spray voltage was set at 4.2 kV and the capillary temperature at 80 °C. EPR spectral data were collected using an X-band Bruker EMX-plus spectrometer equipped with a dual mode cavity at 100 K. GC-MS analysis were recorded on an Agilent 7890B GC system equipped with 5977B MSD Mass analyser.

Synthesis of $[(12\text{-TMC})Co^{II}(ACN)](BF_4)_2$ (1). CH_3CN solution (5 mL) of Cobalt(II) tetrafluoroborate hexahydrate (409 mg, 1.2 mmol) was added to a 20 ml CH_3CN solution of 12-TMC (229 mg, 1 mmol) with constant stirring. The reaction mixture was then refluxed for

12 hours at 80 ºC, and the color of the solution changed to wine red after reaction completion. The reaction mixture was dried over a rotary vacuum and then washed with cold methanol several times to remove excess $[Co^{II}(H_2O)_6](BF_4)_2$. Diethyl ether (50 mL) was added to the resultant semi-solid to precipitate out complex **1** (wine red solid). The precipitate was collected and dried under vacuum over anhydrous $CaCl_2$. To get X-ray quality single crystals, the solid was re-dissolved in CH_3CN layered with diethyl ether and kept at -20 °C, after two days dark brown colored crystals were obtained. Yield: 450 mg (~ 90%). UV: λ_{max} = 485 nm (ε = 170 M^{-1} cm^{-1}). FT-IR (KBr pellet): 2925, 1635, 1475, 1084, 755 cm^{-1}. Mass (*m/z*): Calcd*:* 374.2, Found: 374.2. EPR: Active with low spin (*g = 2.35, 2.31 and 2.05*) Co^{II}-ion (d^7, S = 1/2).

Synthesis of [(12-TMC)$Co^{II}(NO_2)$](BF$_4$) (2). To a 20 ml CH_3CN solution of [(12-TMC)Co^{II}(ACN)]$(BF_4)_2$ (502 mg, 1 mmol), 1 mL aqueous solution of $NaNO_2$ (69 mg, 1 mmol) was added slowly with constant stirring. The mixture was stirred for one hour at RT (298 K) until the color of the solution changed from wine red to light pink indicating completion of the reaction. The volume of the reaction mixture was decreased to 10 mL over rotary vacuum and then layered with diethyl ether and kept for crystallization at -20 °C. Yield: 400 mg (~ 95%). UV: λ_{max} = 535 nm (ε = 24 M^{-1} cm^{-1}). FT-IR (KBr pellet): 2925, 1271, 1084, 755 cm^{-1}. Mass (*m/z*): Calcd*:* 333.1, Found: 333.1.

Synthesis of [(12-TMC)$Co^{II}(^{15}NO_2)$](BF$_4$) (2-$^{15}NO_2$). The synthetic procedure of **2**-$^{15}NO_2$ is similar to that of **2**-$^{14}NO_2$**.** Complex **1** (50.2 mg, 0.1 mmol) dissolved in 5 ml distilled CH_3CN, $Na^{15}NO_2$ (7 mg, 0.1 mmol) was added slowly with constant stirring. The mixture was then stirred for 30 minutes at RT, after reaction completion, the color of the solution changed to dark brown to light pink. The complex was dried under rotary vacuum, washed with cold methanol and diethyl ether, and again dried under vacuum over anhydrous $CaCl_2$. Yield: ~ 35

mg (~ 85%). UV: λ_{max} = 535 nm (ε = 24 M^{-1} cm^{-1}). FT-IR (KBr pellet): 2925, 1245, 1084, 755 cm^{-1}. Mass (*m/z*): Calcd*:* 334.2, Found: 334.2.

Synthesis of complex 4 in the reaction of [(12-TMC)$Co^{II}(NO_2)](BF_4)_2$ + 1 equivalent Acid ($HClO_4$, H^+). Complex **2** with the equimolar amount of perchloric acid ($HClO_4$) in both CH_3CN and H_2O to confirm the reaction product of nitrite reduction reaction. To confirm the end product, complex **2** was reacted with one equivalent of perchloric acid ($HClO_4$, H^+) in CH_3CN at RT under Ar. The color of the above reaction mixture changed to light pink from wine red upon addition of one equivalent H^+, over a time period of one hour, indicating the formation of **4**. The end product, obtained in the reaction of **2** and H^+, was determined to be Co^{III}-NO^- from various spectroscopic and structural characterization. The deep wine red colored crystals were obtained on keeping the solution layered with Et_2O, at -20 °C for 5 days. UV: λ_{max} = 370 nm (ε = 760 M^{-1} cm^{-1}). FT-IR (KBr pellet): 2925, 1703, 1100, 1077 cm^{-1}. Mass (*m/z*): Calcd: 404.2, Found: 404.2 ([(12-TMC)$Co^{III}(NO)(BF_4)]^+$) and calcd: 416.1, Found: 416.1 ([(12-TMC)$Co^{III}(NO)(ClO_4)]^+$). EPR: Silent.

Synthesis of [(12-TMC)$Co^{III}(NO)](BF_4)_2$ (5). The Ar saturated CH_3CN solution (10 mL) containing [(12-TMC)Co^{II}] $(BF_4)_2$ (0.461 g, 1 mmol) was purged with an excess of NO for 5 min; the color of the solution was changed from light pink to wine red color. The reaction mixture was kept for 30 min and then layered with Ar saturated ether. Deep wine red colored crystals [(12-TMC)$Co^{III}(NO)$] $(BF_4)_2$ were obtained by slow diffusion after several days by at -20 °C. UV: λ_{max} = 370 nm (ε = 800 M^{-1} cm^{-1}). FT-IR (KBr pellet): 2925, 1703, 1084 cm^{-1}. Mass (*m/z*): Calcd: 404.2, Found: 404.2 ([(12-TMC)$Co^{III}(NO)(BF_4)]^+$). EPR: Silent. ^{1}H-NMR: active (Figure S6e).

Reactivity Studies. All UV-vis spectral measurements were run in a UV cuvette in CH_3CN or aqueous solutions under Ar at RT. All kinetic reactions were run at least three times, and the

data reported here are the average outcome for these reactions. We have performed all the reaction in the degassed solutions under Ar to avoid the interaction/reaction of dioxygen with nitrosyl /or nitric oxide. Formation of complex **4** and H_2O_2 in the reactions were identified by comparing with authentic samples, and product yields were determined by comparison against standard curves prepared with authentic samples.

Solution IR Spectroscopy. FT-IR grade KBr cells were used to record solution phase IR spectra in Ar saturated CH_3CN at RT. The formation of the complex (**4**), in the reaction of **2** (5.0 mM) with 1 equivalent of $HClO_4$, was followed by monitoring the characteristic $Co^{III}NO^{-}$ stretching. The Co^{II}-bound nitrite peak (1300 cm^{-1}) instantly changed to a new peak 1284 cm^{-1}, which is supposed to be an intermediate (Co^{II}-ONOH, **3**), upon addition of one fold $HClO_4$. The generation of **4** was confirmed by the gradual formation of a peak at 1710 cm^{-1}, characteristic of $Co^{III}NO^{-}$ stretching frequency, with the gradual disappearance of the intermediate peak (1284 cm^{-1}) over a time period of 1 hour.

^{15}N-labeling Experiments by FT-IR Spectroscopy. In addition to solution IR, we have recorded the IR spectra of the different complexes in their solid form as KBr pellet to follow the source of nitrogen. The IR spectra of complex **2** showed a nitrite ($^{14}NO_2^-$) characteristic peak at 1271 cm^{-1}, which shifted to 1245 cm^{-1} when prepared with ^{15}N-labeled nitrite ($^{15}NO_2^-$). The change in the IR stretching frequency of cobalt bound nitrite (Δ = 26 cm^{-1}) confirmed clearly that increase in the reduced mass of nitrogen atom (^{14}N to ^{15}N) is responsible for the decrease in the stretching frequency of nitrite functional group (Fig. S2). We observed the similar spectral changes when the IR spectra of cobalt bound nitrosyl complex recorded with ^{14}N and ^{15}N-labeled cobalt nitrosyl complexes. The IR spectra of complex **4** showed a characteristic nitrosyl stretching frequency at 1703 cm^{-1} (^{14}N) which shifted to 1673 cm^{-1} (^{15}N, Δ = 30 cm^{-1}) when exchanged with ^{15}N-labeled nitrosyl functional group (Fig. S7).

EPR spectroscopy. The EPR spectral measurements were performed to identify/characterized the oxidation state of cobalt metal center in different complexes and to follow the formation of the intermediate (**3**) as well as its conversion to the final $\{CoNO\}^8$ complex (**4**). For EPR spectral measurements, we used the known concentration (2.0 mM) as otherwise required high concentration to detect the EPR signal for cobalt centers with low signal intensity. All EPR spectral measurements were performed in CH_3CN at 100 K under Ar atmosphere. Time-dependent EPR spectra of Co^{II}-ONOH intermediate (**3**; black line) formation and decomposition, in the reaction of complex **2** (2.0 mM) and one equivalent H^+, were recorded in the frozen CH_3CN solutions as a function of time (0, 1, 10, 20, 30, 40, 50, and 60 min) at 100 K.

Nitrite Reduction and ^{15}N-labeling Experiments by ESI-Mass Spectrometry. To establish the source of nitrogen, complex **2** with ^{15}N-labeled nitrite ($[(12\text{-TMC})Co^{II}(^{15}NO_2)]^+$), was reacted with one fold $HClO_4$ in CH_3CN under Ar at 298 K. For above experiment, a schlenk tube (25 mL) containing a solution of **2** (0.5 mM / 10 mL) in CH_3CN sealed with a rubber septum under an Ar was reacted with one fold acid. The reaction mixture was kept for one hour, and then ESI mass spectra of the reaction mixture were recorded.

Qualitative and quantitative estimation of H_2O_2 by ^{1}H-NMR. To confirm the H_2O_2 formation in the reaction of **2** with one fold $HClO_4$, we have monitored the reaction by ^{1}H-NMR spectroscopy. We know that cobalt metal center, being tri-cationic and diamagnetic (low-spin, d^6), in $[(12\text{-TMC})Co^{III}(NO)]^+$ does not participate in the paramagnetic quenching of ^{1}H-NMR signals of attached ligand (12TMC) and H_2O_2. In this regard, the ^{1}H-NMR spectrum of complex **2** (8.4 mg / 500 μL, 40 mM) with one fold $HClO_4$ in CD_3CN showed a signal at 8.66 ppm, corresponds to H_2O_2 (Fig. S11a),. We compared the ^{1}H-NMR spectrum of the H_2O_2 formed in the above reaction with the authentic samples, H_2O_2 only (8.66 ppm; Fig. S12) and

H_2O_2 plus **5** (8.66 ppm; Fig. S11b), which confirmed the formation of H_2O_2 and also validates our hypothesis of H_2O_2 formation in the nitrite reduction chemistry. Additionally, we have calculated the amount of H_2O_2 formation by comparing peak integral corresponding to H_2O_2 (8.66 ppm) of the reaction mixture (**2** + $HClO_4$) with the authentic sample (20 mM H_2O_2 + **5**) containing an internal standard Benzene (8.66 ppm; Fig. S11b). Also, we have observed the formation of 12TMC ligand protons ^{1}H-NMR signals, which suggest the tri-valence and diamagnetic behavior of cobalt center in complex **5** (Fig. S9).

S. No.	Sample	Integral of benzene peak (7.37 ppm) (A)	Integral of H_2O_2 peak (8.66 ppm) (B)	Ratio (B) / (A)
1	20 mM H_2O_2 + **5**	6	4.60	0.766
2	**2** + 1 equiv. H^+	6	2.41	0.402
3	**2** + 1 equiv. H^+	6	2.37	0.395
4	**2** + 1 equiv. H^+	6	2.48	0.410

Amount of H_2O_2 formed:

Sample 1 = (0.402 / 0.766) × 20 mM =10.5 mM (52.5 %)

Sample 2 = (0.395 / 0.766) × 20 mM =10.3 mM (51.5 %)

Sample 3 = (0.410 / 0.766) × 20 mM =10.8 mM (54.0 %)

H_2O_2 formed in the reaction (average): = ~ 53.0 %

Estimation of H_2O_2 (*Iodometric-titration*): Additionally, the amount of hydrogen peroxide was also determined by titration with iodide ion. Hydrogen peroxide was generated in the reaction of complex **2** (250 µL, 1 mM) with one equivalent of perchloric acid (25 µL, 10 mM) in 2.5 mL CH_3CN under an argon atmosphere at room temperature. The reaction solution was treated along with an excess of sodium iodide (100 µL/2.5 mL CH_3CN, 4mM) under argon atmosphere and the UV-visible specrum were recorded for the reaction (Figure S13a). The

quantity of I_3^- formed, in the reaction was determined at 361 nm as a result of I_3^- (λ max 361 nm, ε = 2.5 × 10^4 M^{-1} cm^{-1}) as explained below.

Amount of H_2O_2 formed:

Sample 1 = (Abs. = 1.1) = 0.0324 mM (~ 65 % of H_2O_2)

Sample 2 = (Abs. = 1.05) = 0.0322 mM (~ 64 % of H_2O_2)

Sample 3 = (Abs. = 1.18) = 0.0327 mM (~ 66 % of H_2O_2)

H_2O_2 formed in the reaction (average): = ~ 64.0 %

Also, the generation of hydrogen peroxide in the reaction of complex **2** (250 µL, 1 mM) with four equivalent of perchloric acid (100 µL, 10 mM) was determined under simillar conditions. The reaction solution was treated along with an excess of sodium iodide (100 µL/2.5 mL CH_3CN, 4mM) under argon atmosphere and the UV-visible specrum were recorded for the reaction (Figure S13b).

H_2O_2 formed in the reaction (average): = ~ 55.0 %

The amount of H_2O_2, remaining after the spin trap experiment, was found to be negligible, which was detected by Iodometric test. In this regards, we have reacted complex **2** (1.0 mM) with 2,4-DTBP (1.0 mM) in presence of 1 fold perchloric acid in acetonitrile at RT under Ar. After completion of the reaction, the reaction solution (250 µL, 1 mM) was treated along with an excess of sodium iodide (100 µL/2.5 mL CH_3CN, 4mM) under Ar atmosphere and the UV-visible specrum were recorded for the reaction (Figure S13c). In the trapping reaction, almost all •OH radicals had been consumed by excess 2,4- DTBP to form various 2,4-DTBP derivatives, and hence the formation H2O2 was not observed.

Detection of Co^{II}(ONOH)intermediate (•OH radical trapping experiment): To confirm the N–O bond homolysis and the formation of free •OH radical, we have performed the •OH radical trapping experiment using 2,4-di-tert-butyl phenol (2,4-DTBP). For this reaction, we

have reacted complex **2** (1.0 mM) with 2,4-DTBP (1.0 mM) in presence of 1 fold perchloric acid in acetonitrile at RT under Ar. The reaction mixture was then analysed by GC-MS for identification and amounts quantified by LC against the standard plots of all the compounds. In this experiment, we have observed the formation of 3,5-Di-tert-butylcatechol (3,5-DTBC) with small amounts of 2,4-DTBP-dimer (3,5-DTBP-D) and nitro-2,4-DTBP (nitro-3,5-DTBP) (Figure S14), suggesting the N–O bond homolysis to form free •OH radical and hence indirectly proving the Co^{II}-nitous acid intermediate (**3**). The amount of 3,5-DTBC formed in the reaction was found to be ~ 20 % (0.20 mM), accounting for 40 % •OH radical, 2,4-DTBP-D (~ 10 %, 0.05 mM, 10 % •OH radical), and nitro-2,4-DTBP (~ 5 %, 0.05 mM, 15 % •OH radical) in the reaction mixture, because a specific amount of •OH decomposes to other side products due to its high reactivity.

We have also determined the formation of various products (3,5-DTBC, 3,5-DTBP-D, and nitro-2,4-DTBP) in the reaction of 2,4-DTBP with H_2O_2, in presence and absence of UV light (•OH radical trapping experiment). In this regards, we have reacted 2,4-DTBP (1.0 mM) with H_2O_2 (0.5 mM) in acetonitrile at RT under Ar. The reaction mixture was then analysed and quantified by LC against the standard plots of all the compounds. In this reaction, we observed the formation of the dimerized (3,5-DTBP-D, ~ 20 %) and hydroxylated (3,5-DTBC, ~ 15 %) product mixture in the reaction of 2,4- DTBP with H_2O_2 upon UV exposure. As known from the literature, H_2O_2 generates the •OH radical upon UV light exposure.[XX] However, when the similar reaction was performed in absence of UV light, we did not observe the formation of above reaction mixture.

Single-Crystal XRD Studies. Crystals were mounted on Hampton cryoloops. All geometric and intensity data for the crystals were collected using a Super-Nova (Mo) X-ray diffractometer equipped with a micro-focus sealed X-ray tube Mo-Kα (λ = 0.71073 Å) X-ray

source and HyPix3000 (CCD plate) detector of with increasing ω (width of 0.3 per frame) at a scan speed of either 5 or 10 s/frame. The CrysAlisPro software was used for data acquisition and data extraction. Using Olex2[S3], the structure was solved with the SIR2004[S4] structure solution program using Direct Methods and refined with the ShelXL[S5] refinement package using Least Squares minimisation. All non-hydrogen atoms were refined with anisotropic thermal parameters. Few anions mainly BF_4 ions were found to be highly disordered, and appropriate disordered model applied (Figure S15 and S16). Detail crystallographic data and structural refinement parameters are summarized in Table T1 - T4. CCDC 1900886 (**1**), 1900887 (**2**), 1900888 (**4**), 1882600 (**5**) contains the supplementary crystallographic data for this paper. These data can be obtained free of charge from The Cambridge Crystallographic Data Centre.

Nitric Oxide Preparation and Purification. Nitric oxide (NO) was prepared and purified by following a detailed procedure as shown in Fig. S17. First, NO gas was prepared by the reaction of $NaNO_2$ with H_2SO_4 under an Argon (Ar) atmosphere and then passed through two different types of column. First, pass through a column filled with NaOH beads to remove higher nitrogen oxides impurities. After that, the gas pass through a set of two columns filled with NaOH beads molecular sieves to remove the minor amount of remaining higher nitrogen oxides and moisture impurities. The highly purified NO gas was then collected in a vacuo Schlenk flask fitted with a rubber septum (free from oxygen; after several cycles of vacuum and Ar purging). High pressure NO gas (with pressure >1 atmosphere; the septum bulges outward due to high pressures) then passed through an Ar saturated (oxygen-free) and dry Acetonitrile (CH_3CN) solution for 15 minutes. The concentration of NO in the NO saturated CH_3CN solution is ~14 mM.[S6]

References

S1. Armarego, W. L. F.; Chai, C. L. L. *Purification of Laboratory Chemicals*, 6th ed.; Pergamon Press: Oxford, **2009**.

S2. Halfen, J. A.; Young, V. G., Jr. Efficient Preparation of 1,4,8-trimethylcyclam and its Conversion into a Thioalkyl-pendant Pentadentate Chelate. *Chem. Commun*. **2003**, 2894.

S3 Dolomanov, O. V.; Bourhis, L. J.; Gildea, R. J.; Howard, J. A. K.; Puschmann, H. OLEX2: a Complete Structure Solution, Refinement and Analysis Program. *J. Appl. Cryst*. **2009**, *42*, 339–341.

S4 Burla, M. C.; Caliandro, R.; Camalli, M. C., B.; Cascarano, G. L.; De Caro, L.; Giacovazzo, C.; Polidori, G.; Siliqi, D.; Spagna, R. IL MILIONE: A Suite of Computer Programs for Crystal Structure Solution of Proteins. *J. Appl. Cryst.* **2007**, *40*, 609–613.

S5 G. M. Sheldrick. Crystal Structure Refinement with SHELXL. *Acta Cryst*. **2015**, *C71*, 3–8.

S6. Young, C. L. *Solubility Data Series Val. 8 Oxides of Nitrogen,* International Union of Pure and Applied Chemistry (IUPAC), 1981.

Table T1 Crystallographic data for **1** and **2**.

	1	**2**
Chemical formula	$C_{14}H_{31}B_2CoF_8N_5$	$C_{12}H_{28}BCoF_4N_5O_2$
Formula weight	501.99	420.13
Wavelength /Å	0.71073	0.71073
Crystal system	orthorhombic	orthorhombic
Space group	*P*nma	*P*bca
T, K	293(2)	123(12)
a, Å	14.3880(3)	13.0277(2)
b, Å	8.81800(10)	14.5867(2)
c, Å	16.9008(3)	19.2369(3)
α, °	90	90
β, °	90	90
γ, °	90	90
V/ $Å^3$	2144.26(6)	3655.61(9)
Z	4	8
Calculated density, g/cm^3	1.555	1.527
Abs. Coeff. $/mm^{-1}$	0.879	0.994
Reflections collected	24031	40479
Unique reflections	2499	3981
Refinement method	Least-squares on F^2	Least-squares on F^2
Data/restraints/parameters	2499/0/210	3981/0/230
Goodness-of-fit on F^2	1.047	1.071
Final *R* indices [$I > 2\sigma(I)$]	R1 = 0.0322	R1 = 0.0348
	wR2 = 0.0820	wR2 = 0.0882
R indices (all data)	R1 = 0.0344	R1 = 0.0397
	wR2 = 0.0833	wR2 = 0.0911

Table T2 Selected bond lengths (Å) and bond angles (°) for **1** and **2**.

1		**2**	
Co1 N3	2.023(2)	Co1 O2	2.1208(14)
Co1 N21	1.9838(14)	Co1 O1	2.2098(16)
Co1 N2	1.9838(14)	Co1 N2	2.1813(15)
Co1 N11	1.9836(15)	Co1 N3	2.1781(15)
Co1 N1	1.9836(15)	Co1 N1	2.1562(16)
		Co1 N4	2.2105(16)
N2 Co1 N3	100.39(6)	O2 Co1 O1	57.24(6)
N21 Co1 N3	100.39(6)	O2 Co1 N2	128.27(6)
N21 Co1 N2	87.72(8)	O2 Co1 N3	92.18(6)
N1 Co1 N3	101.19(6)	O2 Co1 N1	131.06(6)
N11 Co1 N3	101.19(6)	O2 Co1 N4	93.03(6)
N11 Co1 N21	88.29(6)	O1 Co1 N4	131.18(6)
N1 Co1 N21	158.43(6)	N2 Co1 O1	90.05(6)
N11 Co1 N2	158.43(6)	N2 Co1 N4	135.41(6)
N1 Co1 N2	88.29(6)	N3 Co1 O1	131.53(6)
N1 Co1 N11	87.67(10)	N3 Co1 N2	81.04(6)
		N3 Co1 N4	81.44(6)
		N1 Co1 O1	91.44(6)
		N1 Co1 N2	82.68(6)
		N1 Co1 N3	133.61(6)
		O1 N5 O2	112.05(16)
		N1 Co1 N4	80.47(6)
		N5 O2 Co1	97.31(11)
		N5 O1 Co1	93.35(12)

Table T3 Crystallographic data for **4** and **5**.

	4	**5**
Chemical formula	$C_{12}H_{28}B_2CoF_8N_5O$	$C_{12}H_{28}CoN_5OB_2F_8$
Formula weight	490.94	490.94
Wavelength /Å	0.71073	0.71073
Crystal system	orthorhombic	orthorhombic
Space group	*Pna21*	*P*na21
T, K	293(2)	293(2)
a, Å	12.8109(4)	12.8109(4)
b, Å	18.5996(6)	18.5996(6)
c, Å	8.9913(3)	8.9913(3)
α, °	90	90
β, °	90	90
γ, °	90	90
V/ $Å^3$	2142.43(12)	2142.43(12)
Z	4	4
Calculated density, g/cm^3	1.522	1.522
Abs. Coeff. $/mm^{-1}$	0.881	0.881
Reflections collected	18328	18328
Unique reflections	3701	3701
Refinement method	Least-squares on F^2	Least-squares on F^2
Data/restraints/parameters	3701/46/390	3701/187/374
Goodness-of-fit on F^2	1.049	1.058
Final *R* indices [$I > 2\sigma(I)$]	R1 = 0.0487	R1 = 0.0541
	wR2 = 0.1260	wR2 = 0.1434
R indices (all data)	R1 = 0.0707	R1 = 0.0758
	wR2 = 0.1429	wR2 = 0.1611

Table T4 Selected bond lengths (Å) and bond angles (°) for **4** and **5.**

4		**5**	
Co1 N5	1.753(6)	Co1 N1	2.002(11)
Co1 N1	2.010(10)	Co1 N2	1.965(12)
Co1 N2	1.987(11)	Co1 N5	1.744(6)
Co1 N3	1.961(11)	Co1 N3	1.984(12)
Co1 N4	1.961(11)	Co1 N4	1.977(11)
N5 Co1 N1	101.2(6)	N2 Co1 N1	88.4(6)
N5 Co1 N2	103.4(6)	N5 Co1 N1	101.1(7)
N5 Co1 N3	103.2(6)	N5 Co1 N2	104.5(6)
N5 Co1 N4	101.2(6)	N5 Co1 N3	103.3(6)
N2 Co1 N1	88.4(6)	N5 Co1 N4	100.3(7)
N3 Co1 N1	155.5(4)	N3 Co1 N1	155.6(4)
N3 Co1 N2	87.6(2)	N3 Co1 N2	87.5(2)
N4 Co1 N1	86.4(2)	N3 Co1 N4	87.4(7)
N4 Co1 N2	155.4(4)	N4 Co1 N1	86.26(19)
N4 Co1 N3	87.3(6)	N4 Co1 N2	155.2(5)
O9 N5 Co1	137(4)	O9 N5 Co1	134.7(7)

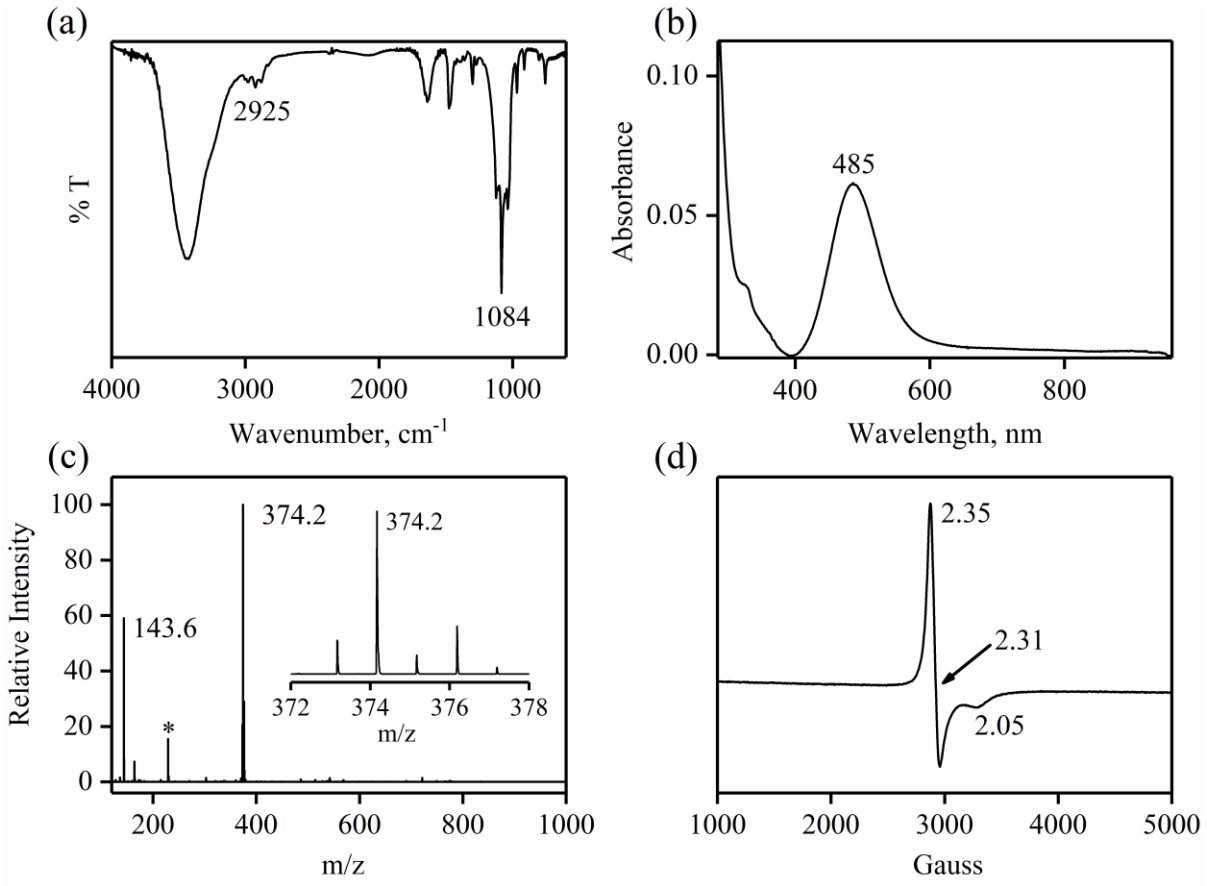

Fig. S1. (a) FT-IR spectrum of **1** recorded in KBr pellet at 298 K, showing the peaks for aliphatic chain (2925 cm^{-1}) and tetrafluoroborate (1084 cm^{-1}) (b) UV-vis spectrum of **1** (0.50 mM) recorded in CH_3CN at 298 K. Spectrum showing here the characteristic absorption band at 485 nm for complex **1**. (c) ESI-MS spectrum of **1** recorded in CH_3CN. The peaks at *m/z* 143.6 and 347.2 are assigned to be $[(12\text{-TMC})Co^{II}]^{2+}$ (calcd: *m/z* 143.6) and $[(12\text{-TMC})Co^{II}(BF_4)]^{+}$ (calcd: *m/z* 374.2), respectively. The peak at *m/z* 229.2 marked with asterisks is assigned to be protonated 12-TMC ligand $[12\text{-TMCH}]^{+}$ (calcd: *m/z* 229.2) (d) X-band EPR spectra of **1** (2.0 mM; black line) recorded at 100 K.

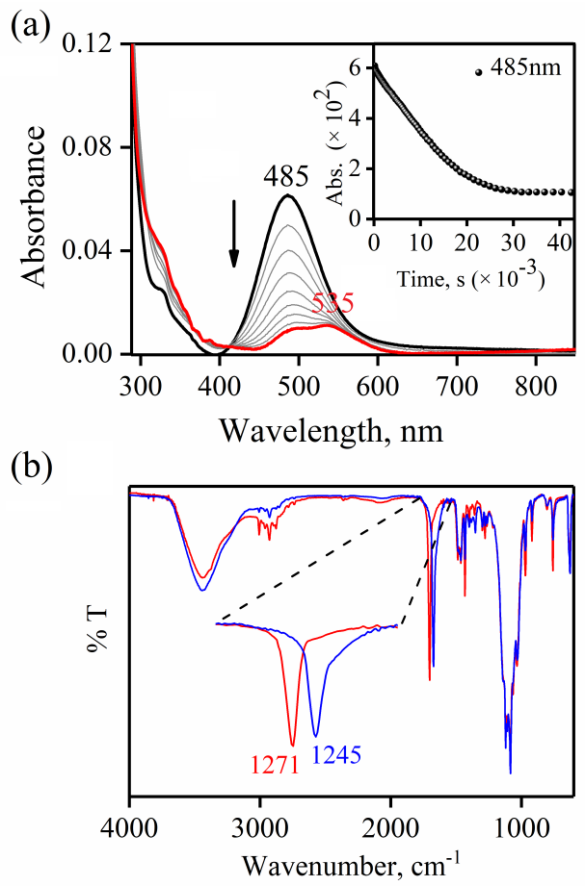

Fig. S2. (a) UV-vis spectra for the formation of **2**. The Inset shows the time course of the decay of **1** (black circles) monitored at 485 nm upon addition $NaNO_2$ (1 equiv) to a solution of **1** (0.5 mM) in CH_3CN at 298 K. (b) FT-IR spectra of $[(12\text{-TMC})Co^{II}(^{14}NO_2)]^+$ (red line) and $[(12\text{-TMC})Co^{II}(^{15}NO_2)]^+$ recorded in KBr pellet at 298 K.

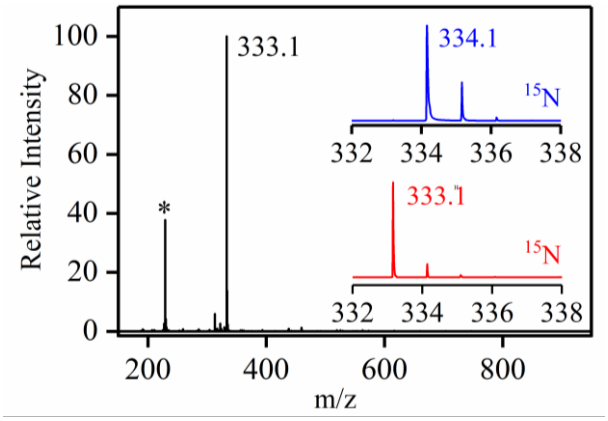

Fig. S3. ESI-MS spectrum of **2** recorded in CH_3CN. The peak at *m/z* 334.1 and *m/z* 229.2 (*) are assigned to be $[(12\text{-TMC})Co^{II}(^{14}NO_2)]^{2+}$ (calcd: *m/z* 331.1) and protonated 12-TMC ligand $[12\text{-TMCH}]^+$ (calcd: *m/z* 229.2). Inset: isotopic distribution pattern for **2**-$^{14}NO_2^-$ (red line) and **2**-$^{15}NO_2^-$ (blue line).

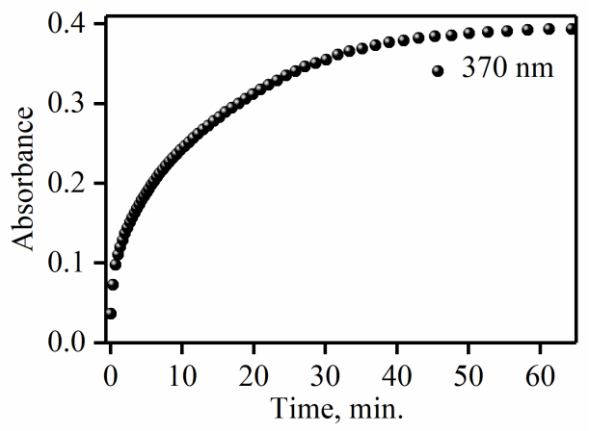

Fig. S4. Time course of the formation of **4** (black circles) monitored at 370 nm upon addition $HClO_4$ (H^+, 1 equivalent) to a solution of **2** (0.5 mM) in CH_3CN at 298 K.

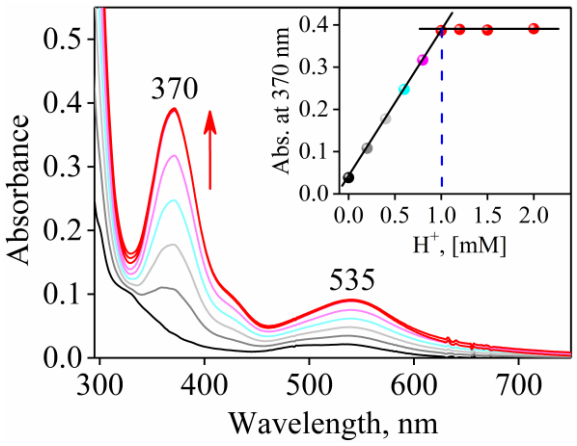

Fig. S5. (a) UV-vis spectral changes showing the formation of **4** (black line) by addition of $HClO_4$ (H^+ source) in increments of 0, 0.20, 0.40, 0.60, 0.8, 1.0, 1.2, 1.5, 2.0 equivalents under an Ar atmosphere in CH_3CN at 298 K. The Inset shows the spectral titration monitored at 370 nm due to the formation of **4** as a function of the equivalents of $HClO_4$ (H^+ source) in increments of 0, 0.20, 0.40, 0.60, 0.8, 1.0, 1.2, 1.5, 2.0 equivelents.

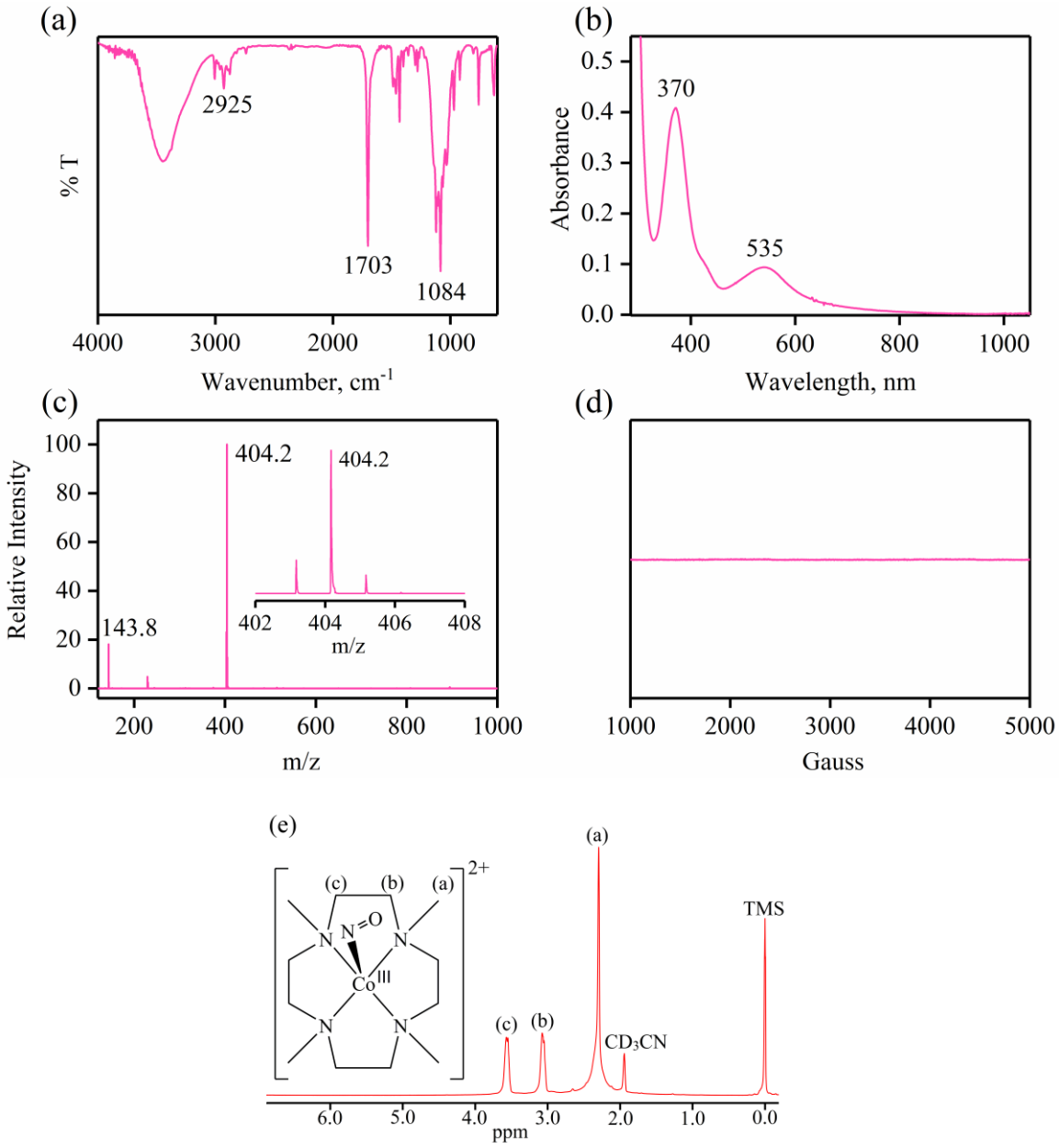

Fig. S6. (a) FT-IR spectrum of **5** recorded in KBr pellet at 298 K. The spectrum showed the peaks for aliphatic chain (2925 cm^{-1}), $Co^{III}NO^{-}$ (1703 cm^{-1}), and for BF_4^- (1084 cm^{-1}). (b) UV-vis spectrum of **5** (0.50 mM) recorded in CH_3CN at 298 K. Spectrum showing here the characteristic absorption band at 370 nm for complex **5**. (c) ESI-MS spectrum of **5** recorded in CH_3CN. The peaks at *m/z* 143.8 and 404.2 are assigned to be $[(12\text{-TMC})Co^{II}]^{2+}$ (calcd: *m/z* 143.6) and $[(12\text{-TMC})Co^{II}(NO)(BF_4)]^{+}$ (calcd: *m/z* 404.2), respectively. (d) X-band EPR spectrum of **5** (2.0 mM) recorded at 100 K. (e) ^{1}H-NMR (400 MHz) spectra of complex **5** (40 mM) in CD_3CN at RT.

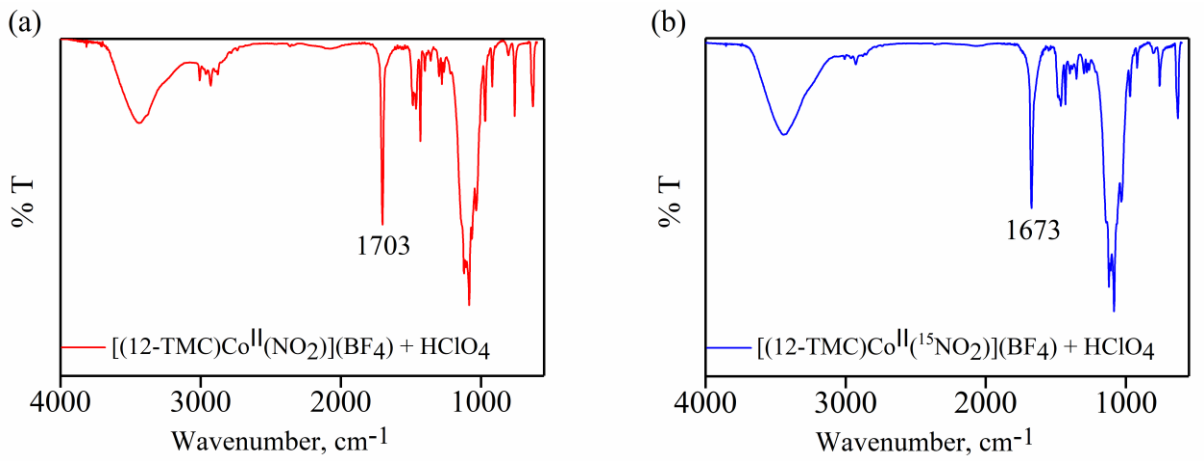

Fig. S7. FT-IR spectrum of (a) reaction mixture, ([(12-TMC)Co^{II}($^{14}NO_2$)]$^{2+}$, 40 mM + $HClO_4$, 40 mM), recorded after completion of reaction in KBr pellet at 298 K. The spectrum showed the peaks for aliphatic chain (2925 cm^{-1}), {$Co^{14}NO$}^{8} (1703 cm^{-1}), and addition peak for ClO_4^- + BF_4^- (1050 to 1180 cm^{-1}). (b) Reaction mixture, ([(12-TMC)Co^{II}($^{15}NO_2$)]$^{2+}$, 40 mM + $HClO_4$, 40 mM), recorded after completion of reaction in KBr pellet at 298 K. The spectrum showed the peaks for aliphatic chain (2925 cm^{-1}), {$Co^{15}NO$}^{8} (1673 cm^{-1}), and addition peak for ClO_4^- + BF_4^- (1050 to 1180 cm^{-1}).

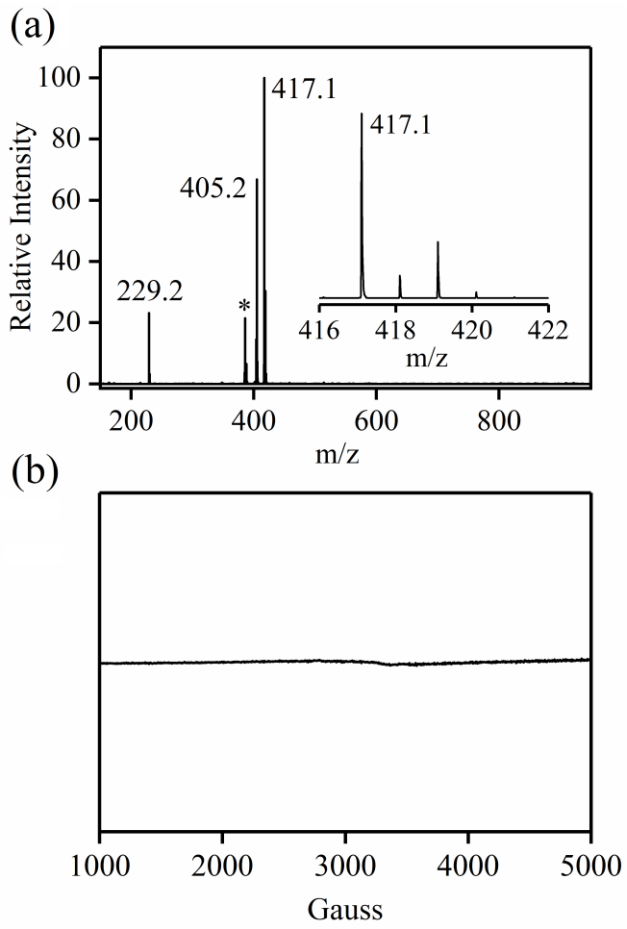

Fig. S8. ESI-MS spectrum of **4** recorded in CH_3CN. The peaks at *m/z* 229.2, 405.2 and 417.1 are assigned to be protonated 12-TMC ligand $[12\text{-TMCH}]^+$ (calcd *m/z* 229.2), $[(12\text{-TMC})Co^{III}(^{15}NO)(BF_4)]^+$ (calcd *m/z* 405.2) and $[(12\text{-TMC})Co^{III}(^{15}NO)(ClO_4)]^+$ (calcd *m/z* 417.1), respectively. The peak at *m/z* 386.1 marked with asterisks is assigned to be protonated 12-TMC ligand $[(12\text{-TMC})Co^{II}(ClO_4)]^+$ (calcd *m/z* 386.1). (b) X-band EPR spectrum of **5**-^{14}NO (2.0 mM) recorded at 100 K.

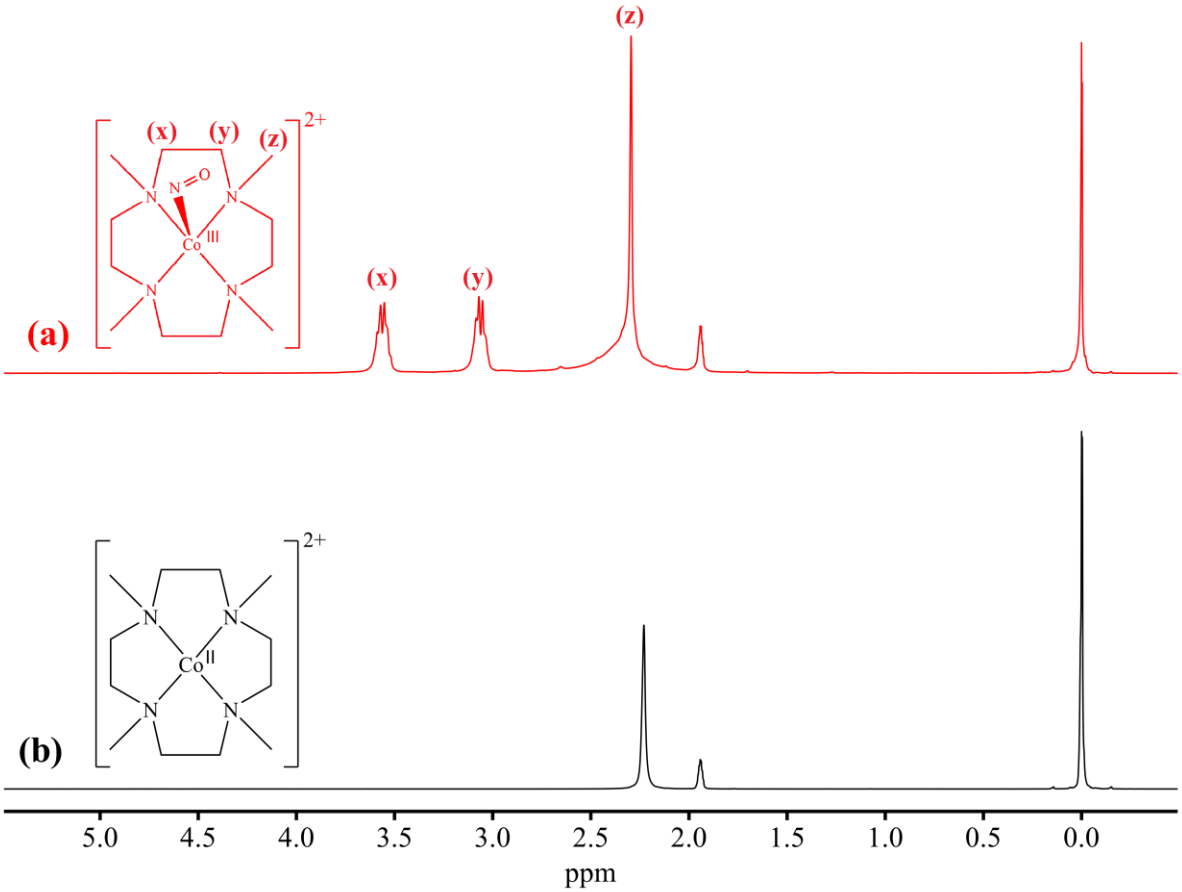

Fig. S9. ^{1}H-NMR (400 MHz) spectra of (a) reaction mixture (**2**, 40 mM + $HClO_4$, 40 mM) and (b) complex **1** (40 mM) in CD_3CN at RT.

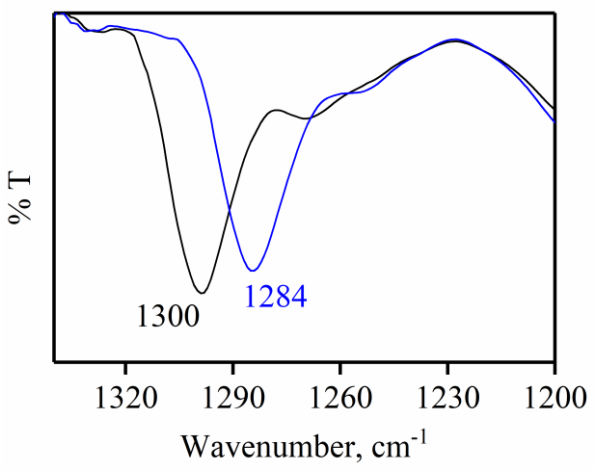

Fig. S10. Solution IR spectra of $[(12\text{-TMC})Co^{II}(NO_2)]^+$ (**2**, black line) and $[(12\text{-TMC})Co^{II}(ONOH)]^+$ (**3**, blue line) recorded in CH_3CN at 298 K.

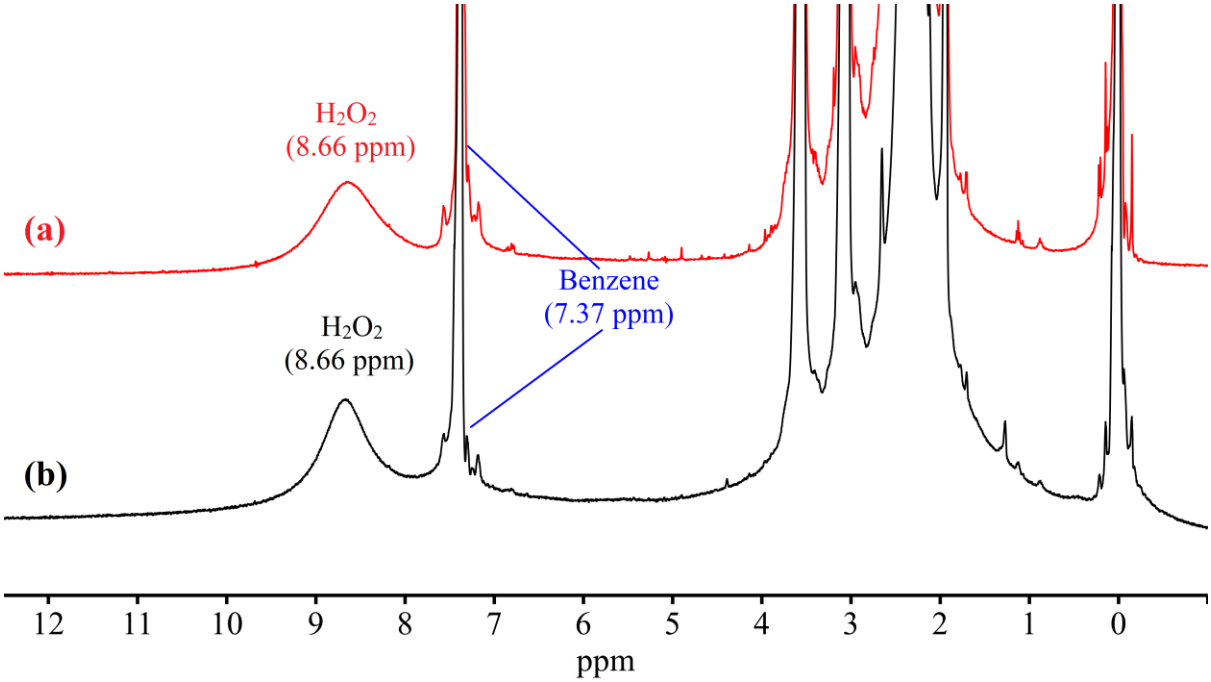

Fig. S11. ^{1}H-NMR (400 MHz) spectra of (a) reaction mixture (**2**, 40 mM + $HClO_4$, 40 mM) and (b) authentic sample (H_2O_2, 20 mM + **5**, 40 mM) using benzene as an internal standard in CD_3CN at RT.

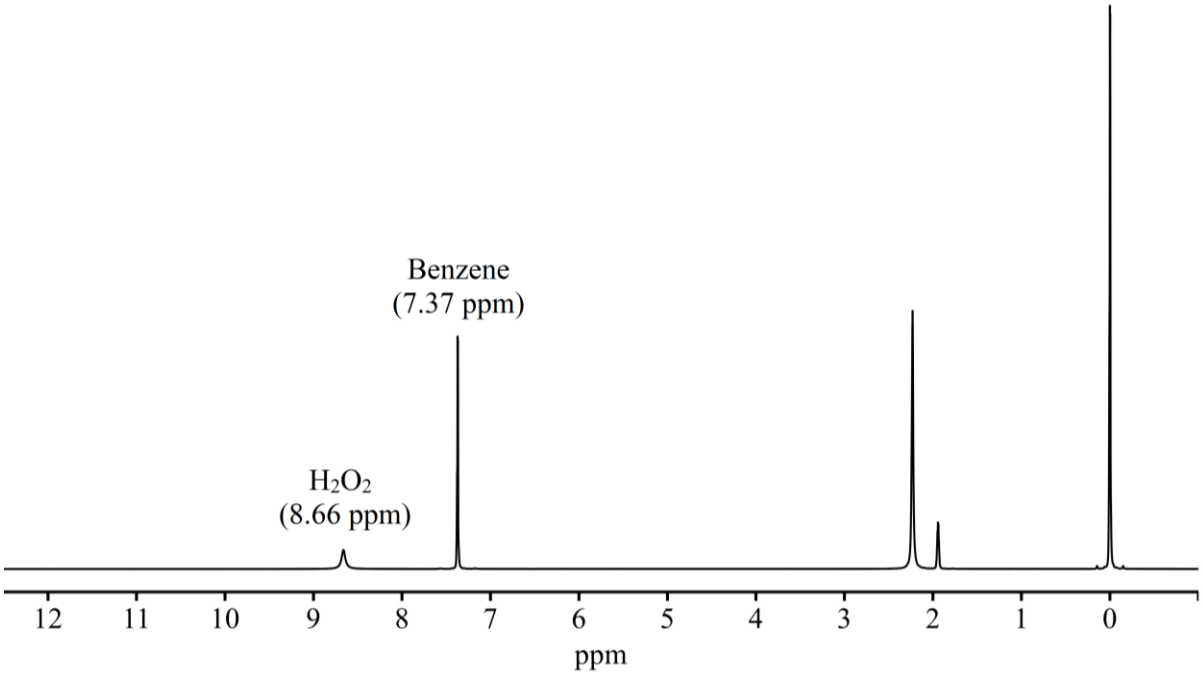

Fig. S12. ^{1}H-NMR (400 MHz) spectra of H_2O_2 (20 mM) using benzene as an internal standard in CD_3CN at RT.

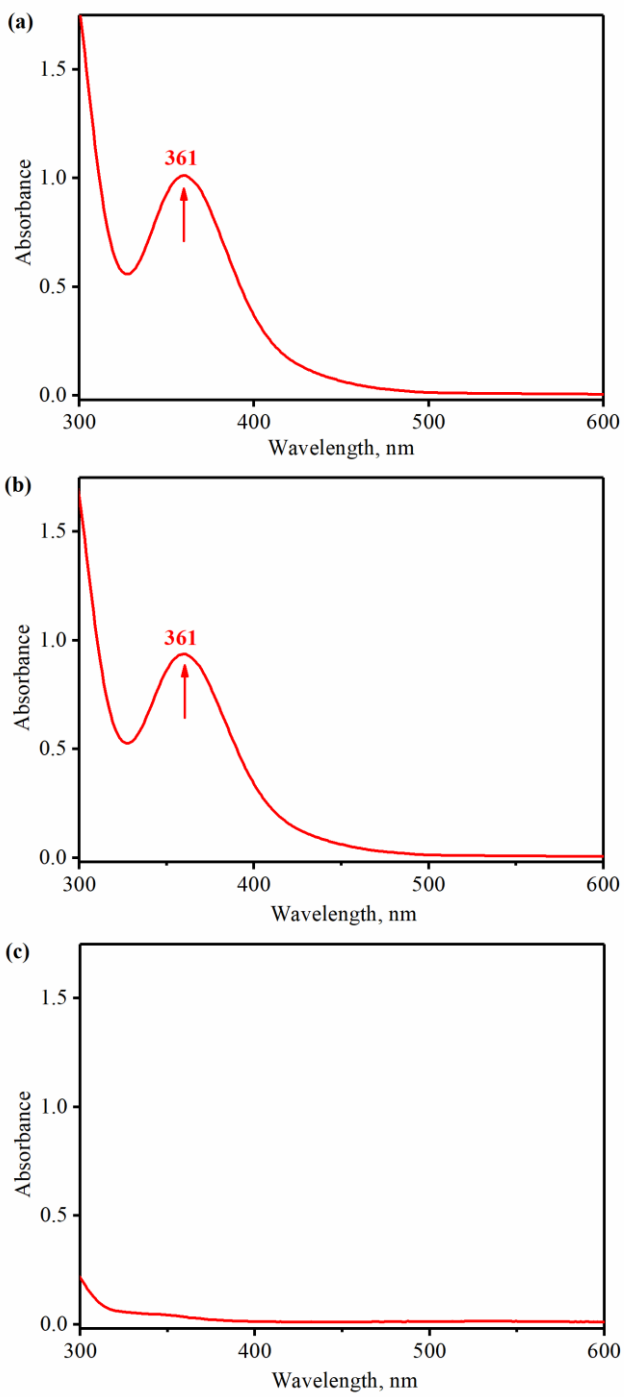

Fig. 13. (a) UV-vis spectrum complex **2** (0.01 mM) with one equivalent of perchloric acid (0.01 mM) in CH_3CN under an Ar atmosphere at 298 K. (b) UV-vis spectrum of complex **2** (0.01 mM) with 4 equivalent of perchloric acid (0.04 mM) in CH_3CN under an Ar atmosphere at 298 K. (c) UV-vis spectrum of reaction mixture (0.01 mM) obtained after the spin trapping experiment in CH_3CN under an Ar atmosphere at 298 K.

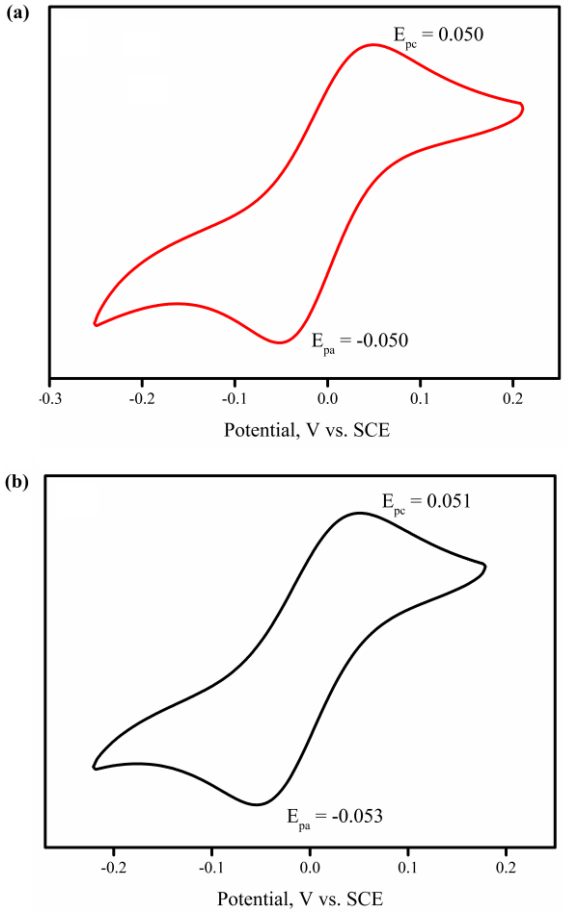

Fig. S14. Cyclic voltammogram of (a) **4** (5.0 mM) and (b) **4** (5.0 mM) + H_2O_2 (2.5 mM) in CH_3CN containing n-Bu_4NClO_4 (0.1 M) as a supporting electrolyte (scan rate = 0.10 V s^{-1}).

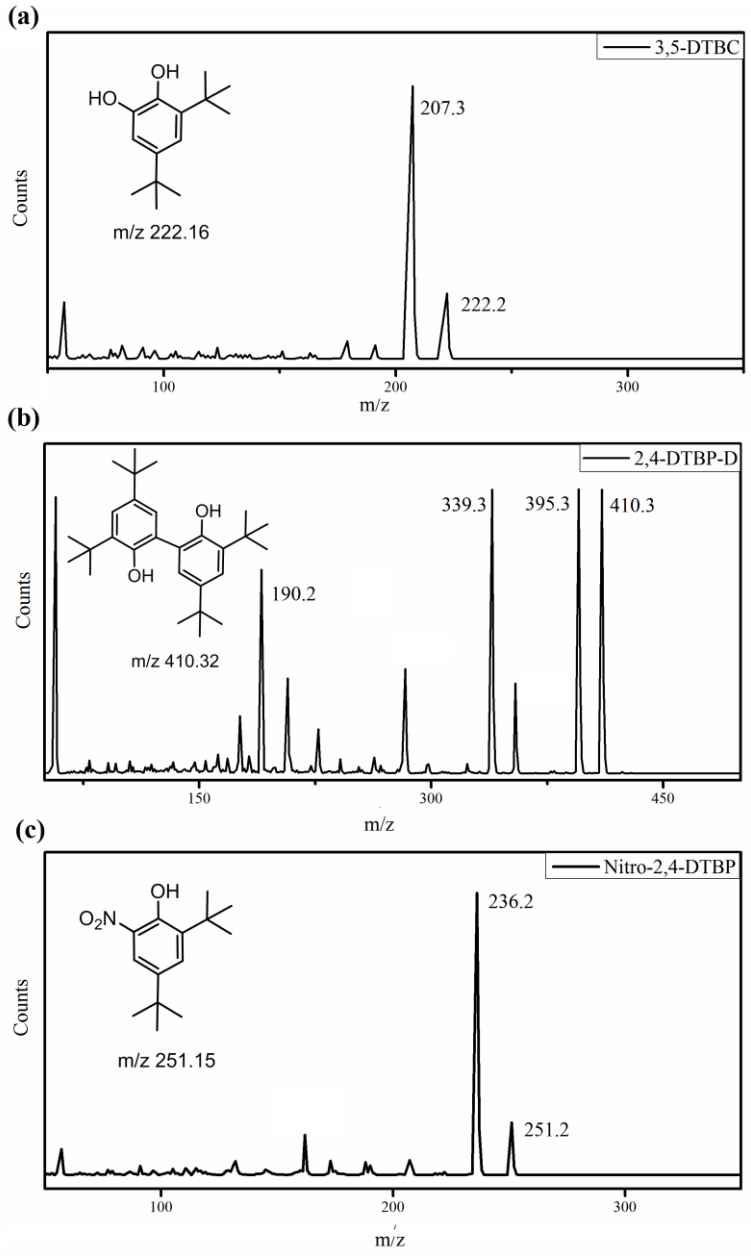

Fig. S15. GC-MS characterisation of (a) 3,5-Di-*tert*-butylcatechol (3,5-DTBC); The peak at *m/z* value 222.2, 207.3 are assigned to 3,5-DTBC and CH_3 loss from 3,5-DTBC respectively. (b) 2,4-DTBP-dimer (2,4-DTBP-D); The peaks at *m/z* 410.3, 395.3, 339.3 and 190.2 are assigned to be 2,4-DTBP-D, loss of CH_3 from 2,4-DTBP-D, loss of C_4H_8 and CH_3 from 2,4-DTBP-D and loss of CH_3 from monomer 2,4-DTBP (c) nitro-2,4-DTBP (nitro-2,4-DTBP): The peaks at *m/z* 251.2 and 236.2 are assigned to be nitro-2,4-DTBP and loss of CH_3 from nitro-2,4-DTBP . The peaks were compared with the NIST standard library.

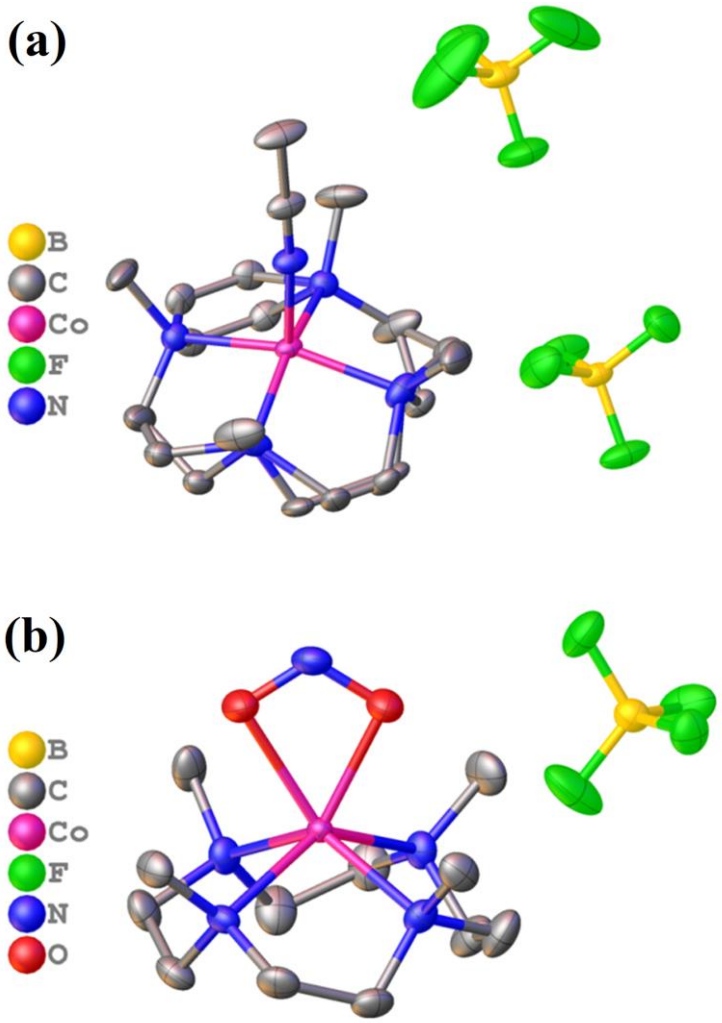

Fig. S16: ORTEP diagram of **1** (a) and **2** (b) with 30 % probability. The disordered portions in the anions are removed for clarity.

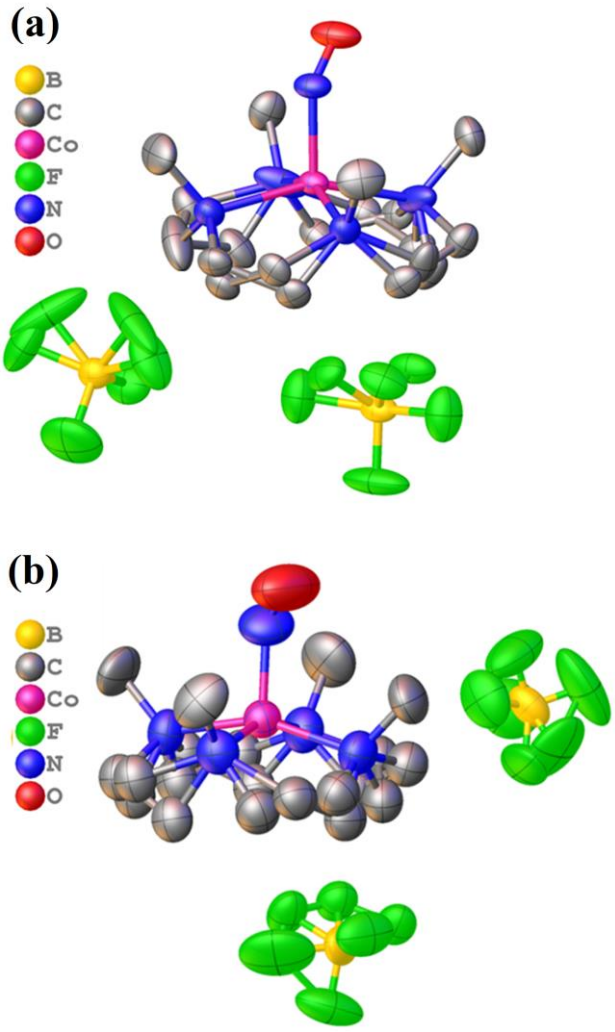

Fig. S18: ORTEP diagram of **4** (a) and **5** (b) with 30 % probability. The disordered portions in the anions of BF_4 are removed for clarity.

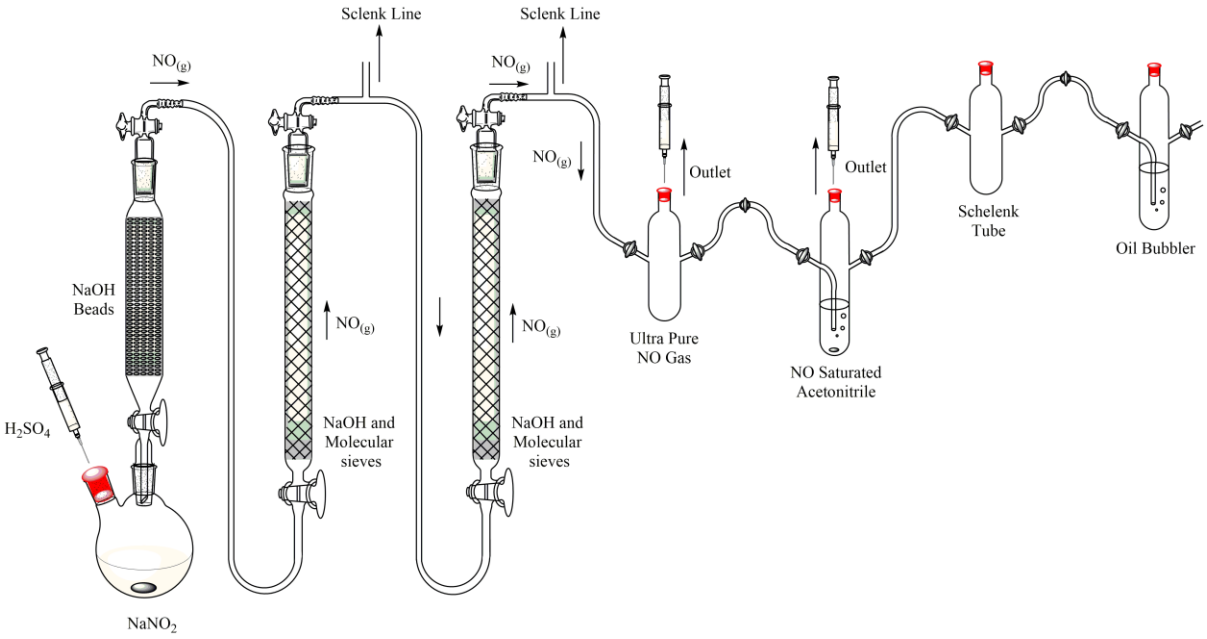

Fig. S19. Schematic diagram showing the generation and purification setup for NO.